Mass transport through vertically aligned large diameter MWCNTs embedded in parylene

Mass transport through vertically aligned large diameter MWCNTs embedded in parylene

P Krishnakumar[1], P B Tiwari[2], S Staples[1], T Luo[1], Y Darici[2], J He[2] and S M Lindsay[1,3,4]

[1] Department of Physics, Arizona State University, Tempe, AZ 85287, USA
[2] Department of Physics, Florida International University, Miami, FL 33199, USA
[3] Biodesign Institute, Arizona State University, Tempe, AZ 85287, USA
[4] Department of Chemistry and Biochemistry, Arizona State University, Tempe, AZ 85287, USA

E-mail: jinhe@fiu.edu and Stuart.Lindsay@asu.edu

Abstract

We have fabricated porous membranes using a parylene encapsulated vertically aligned forest of multi-walled carbon nanotubes (MWCNTs, about 7 nm inner diameter). The transport of charged particles in electrolyte through these membranes was studied by applying electric field and pressure. Under an electric field in the range of 4.4×10^4 V m^{-1}, electrophoresis instead of electroomosis is found to be the main mechanism for ion transport. Small molecules and 5 nm gold nanoparticles can be driven through the membranes by an electric field. However, small biomolecules, like DNA oligomers, cannot. Due to the weak electric driving force, the interactions between charged particles and the hydrophobic CNT inner surface play important roles in the transport, leading to enhanced selectivity for small molecules. Simple chemical modification on the CNT ends also induces an obvious effect on the translocation of single strand DNA oligomers and gold nanoparticles under a modest pressure (<294 Pa).

[S] Online supplementary data available from stacks.iop.org/Nano/23/455101/mmedia

(Some figures may appear in colour only in the online journal)

1. Introduction

In recent years, there has been enormous interest in utilizing carbon nanotubes as nanochannels or nanopores [9, 20, 27, 22, 35, 11, 7, 8]. From a biological point of view, the CNT is an ideal model to help understand the transporter proteins on the cell membrane that work in aqueous environments with hydrophobic inner walls and nanometer channel sizes. From the point of view of fundamental research, it is an exciting system in which to test classical theories of fluid mechanics and dynamics at the nanoscale, especially below 10 nm. CNTs have several advantages as nanopores or nanochannels. (1) They require no special nanofabrication to achieve a pore size of molecular size (ranging from less than 1 nm to more than 10 nm). They have an atomically smooth surface and perfect uniformity over large distances, resulting in

frictionless motion of fluid and particles. Recent studies have observed significantly faster transport in CNTs compared with nanochannels made from conventional materials [7, 37, 8, 17]. (2) For high quality CNTs, the chemistry and structures of the interior surface are well defined, which simplifies theoretical simulations. (3) The excellent electrical properties of CNTs provide new routes to electrical detection, trapping and manipulation of charged biomolecules and nanoparticles. (4) Well defined sites are available for chemical functionalization at the ends of the tubes. Such modifications will be extremely useful for ion and molecule selection, gating or separation. To develop a fundamental understanding of mass transport inside CNTs, transport measurement based on single SWCNTs (diameter < 2 nm) has been developed in recent years [15, 31, 26]. However, the individual CNT based nanofluidic device is difficult to fabricate and the measurement results

are still limited. Currently, measurements of mass and charge transport in the CNT are made mainly with membranes containing a large quantity (i.e. 10^{9-11} tubes cm^{-2}) of CNTs, the orientation of which is either aligned or not aligned [8, 19, 37, 32]. The membranes with aligned CNTs generally show better performance. However, it is difficult to grow high quality aligned CNTs with diameters below 2 nm [8, 37]. Various polymers have been cast onto the CNT film to fill the gaps between CNTs and form an impenetrable membrane. Subsequently, both ends of the CNT were opened by oxygen plasma. Recent research on CNT based nanofluidic devices has yielded exciting applications in efficient gas filtration, chemical and biological separation, water desalination and programmable transdermal drug delivery [4, 2, 38].

We have fabricated vertically aligned MWCNT membranes (about 7 nm in tube inner diameter and 42 μm in tube length) by depositing parylene on a vertically aligned MWCNT forest. The parylene deposition process is simple, reproducible and compatible with current microfabrication techniques. Parylene film is chemically inert, electrically resistive and pin-hole free and has low permeability to moisture and gases. Parylene is also known for its capability to conformally cover all surfaces regardless of the configuration of the surface, including configurations with high aspect ratio [3, 21]. MWCNT forests embedded in parylene have been used in several applications, including electrochemical sensors [21, 1, 34], but not as a membrane for mass transport. Although there are several different methods for fabricating CNT membranes, new CNT membrane geometries will always provide new insight into the mass and charge transport in CNTs due to the heterogeneous physical properties of CNTs and the complexity of CNT based nanofluidics. Here, we report measurements using this new type of CNT membrane to help improve our understanding of several aspects, as follows. (1) The transport of particles through CNTs under electric field. Pressure and electric field are often used to drive particles through the CNTs [19]. Diffusion due to a concentration gradient is normally not efficient for these CNT membranes because of the extremely small pore diameter and surface interactions. Pressure driven gas, fluid flow and small particle transport through CNT membranes have been investigated extensively [22, 8, 19, 17, 7]. In contrast, there are only a few studies of electric field driven particle transport [32, 37]. (2) The effect of CNT diameter, length and electrostatic environment to the particle transport under electric field. In electrolyte, the applied electric field will drive the transport of charged particles by both electrophoresis and electroosmosis. Electrophoretic flow is proportional to the external electric field, the particle mobility and the ion concentration. The electrophoretic flow only increases moderately (i.e. several-fold) with a decrease of CNT diameter [24, 37]. Electroosmotic flow is proportional to the external electric field, the fluid velocity and the net (unbalanced) charge density of the fluid inside the channel. The fluid velocity is sensitive to the slip boundary condition at the CNT inner surface. The net charge density is directly affected by charge selection at the entrances and the surface charge density at the CNT inner surface.

Electroosmosis is more sensitive to the CNT diameter than electrophoresis. Greatly enhanced electroosmosis (i.e. several orders of magnitude) has been observed in smaller diameter SWCNTs [24] due to increased slip length at smaller diameter and increased net charge density inside smaller diameter CNTs. Electroosmosis has been used as an efficient pump to drive ions and small molecules (charged or neutral) through small diameter SWCNTs. However, as suggested by simulations and experiments, electroosmosis is much weaker in larger diameter CNTs. In addition, the CNT length and electrostatic environment will also affect electroosmosis and electrophoresis differently. So the motion of particles under an electric field is complicated and depends on the specific conditions. (3) Most of the previous works focused on the transport of gas molecules, water, ions and small molecules. The transport of biomolecules has not been well studied in these CNT membranes. In this report, the translocation of small molecules, DNA and nanoparticles is studied, especially driven by an electric field. Molecule–carbon surface interactions are found to play important roles in the transport of these particles. Furthermore, chemical modifications on the MWCNT membrane also strongly affect the transport of large particles across the membrane.

2. Experimental methods

2.1. MWCNT forest growth and characterization

A 30 nm thick aluminum layer and 1 nm thick iron layer were deposited sequentially on a silicon chip containing a silicon nitride membrane (see section 2.2) using ion-beam sputtering or electron-beam deposition. The vertically aligned MWCNT forest was grown from this catalyst by chemical vapor deposition (CVD) using ethylene as the carbon source at 850 °C for 70 s [8]. A scanning electron microscope (SEM) image of the as-grown vertically aligned MWCNT forest is shown in figure 1(a). The height of the CNT forest is about 42 ± 5 μm under our growth conditions. The inset in figure 1(b) shows a transmission electron microscope (TEM) image of individual CNTs, confirming that these CNTs are multi-walled (∼5–10 layers) and the inner and outer diameters are about 7 nm and 11 nm respectively. Bamboo structure is not observed in these MWCNTs. By analyzing more than 100 CNTs in TEM images, we obtained a histogram (figure 1(b)) of the CNT inner diameter distribution, with the peak around 7 nm. These carbon nanotubes were also characterized by Raman spectroscopy, confirming MWCNT structures (figure S1 available at stacks.iop.org/Nano/23/455101/mmedia).

2.2. Parylene coated MWCNT forest membrane fabrication

The fabrication of the vertically aligned MWCNT forest membrane is based on the procedure developed by Holt *et al* [8]. In brief, a 5 mm square silicon chip with a square shaped free standing silicon nitride membrane (35–100 μm in width, 300 nm in thickness) in the center is first fabricated by potassium hydroxide (KOH) anisotropic wet etching. After the MWCNT forest is grown uniformly on the whole
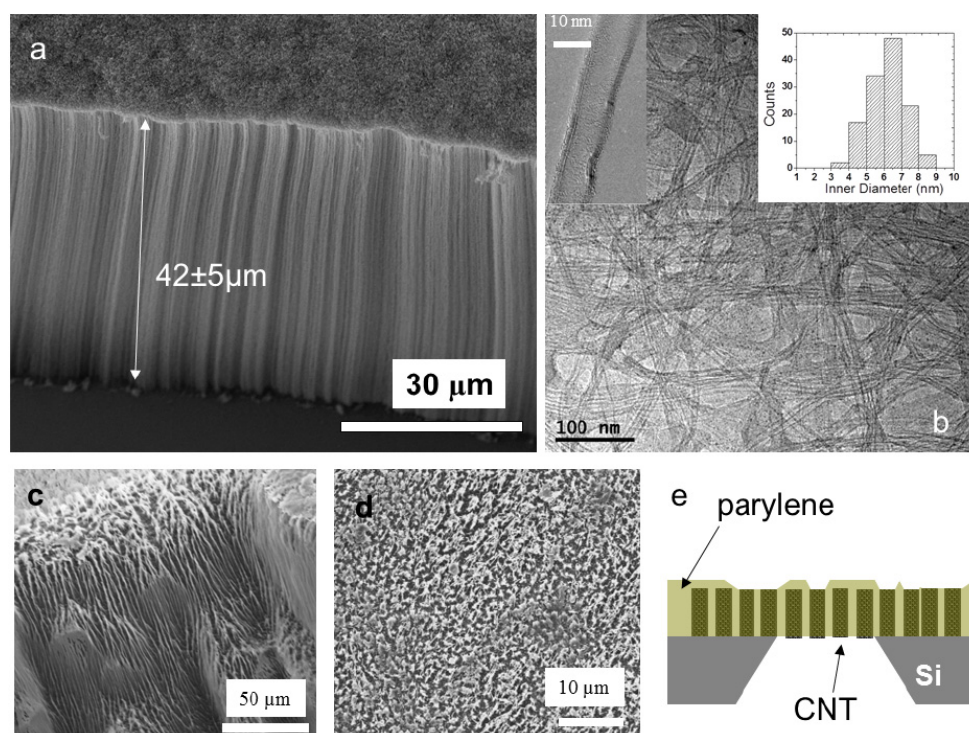
Figure 1. (a) SEM image of a cross-section of the as-grown vertically aligned MWCNT forest. The average height of the CNT forest is about 42 μm. (b) Low resolution TEM image of a large number of MWCNTs. The inset in the top left corner is a high resolution TEM image of one MWCNT. The inset in the top right corner shows the histogram of inner diameters of these MWCNTs. (c) A SEM image shows the cross-section of the parylene coated MWCNT membrane. (d) A SEM image shows the membrane surface after oxygen plasma treatment. (e) A schematic diagram of the parylene encapsulated MWCNT forest membrane on a silicon support with a square window with size 35–100 μm.

surface, parylene is vapor deposited onto the MWCNT forest at room temperature using a PDS 2010 LABCOTER (Specialty Coating Systems, Indianapolis, IN). Immediately after deposition, the parylene film is planarized by thermal annealing at 350 °C for 2 h in argon atmosphere [28]. SEM images in figure 1(c) suggest that the CNT forests are fully embedded in parylene. A two-step reactive ion etching (RIE) process is used to sequentially remove the excess parylene film and the 300 nm SiN layer from the backside of the chip. Then the chip is sequentially immersed in 45 °C PAN etch solution (H_3PO_4:H_2O:HNO_3:CH_3COOH) (16:2:1:1, volume ratio) for 5 min and in HCl (50% of concentrated HCl) for 30 min, to remove the exposed Al and Fe layers from the backside. Then oxygen plasma (2–4 min, 7.2 W, 550–600 mTorr) is used to remove the excess parylene, and to expose and open the CNT ends. The surface of the membrane after oxygen plasma is shown in figure 1(d). The as-grown parylene surface is hydrophobic. However, the parylene surface becomes hydrophilic after oxygen plasma treatment. The hydrophilic parylene surface is stable and facilitates the transport of particles. A schematic diagram of the final device is shown in figure 1(e). We have also measured the porosity of a CNT membrane (after 3 min oxygen plasma treatment) using a KCl diffusion method [19]. A pore area of 7.2×10^{-11} m^2 and porosity of 0.89% is obtained for one of the CNT membranes. Based on the average CNT diameter (7 nm), we obtained a CNT area density of 0.23×10^{11} cm^{-2}. This is in line with estimates by other groups [41, 7] but

subject to considerable uncertainty—for example, the pore diameter estimated from the membrane conductance is about a factor three too large (an error that may also reflect enhanced ion mobility in the interior of the CNTs).

Some of the MWCNT membranes are chemically modified. The MWCNT membranes are immersed in aqueous solution composed of 20 mM EDC and 20 mM of sulfo-NHS for 2 h at room temperature. Then the membranes are rinsed by H_2O and immersed in 20 mM ethanolamine hydrochloride for 20 min. The parylene film is also modified by ethanolamine, as demonstrated by contact angle measurements (figure S4(b) available at stacks.iop.org/Nano/23/455101/mmedia).

2.3. Materials, chemical reagents and solution preparation

5 and 10 nm gold nanoparticles (NPs) were purchased from Ted Pella. These gold nanoparticles are capped with negative citrate ligand and the size is very accurate, with only 10% size variation. No aggregation is observed when these particles are dissolved in pure water or aqueous solution with low salt concentration (<15 mM KCl solution) [5]. A single strand DNA oligomer (GTCGTCGTCGTC) was obtained from IDT (Integrated DNA Technologies). Other chemical reagents were purchased from Sigma Aldrich and used without further purification. All solutions were prepared using deionized (DI) water (~18 MΩ) from a water purification system (Ultra
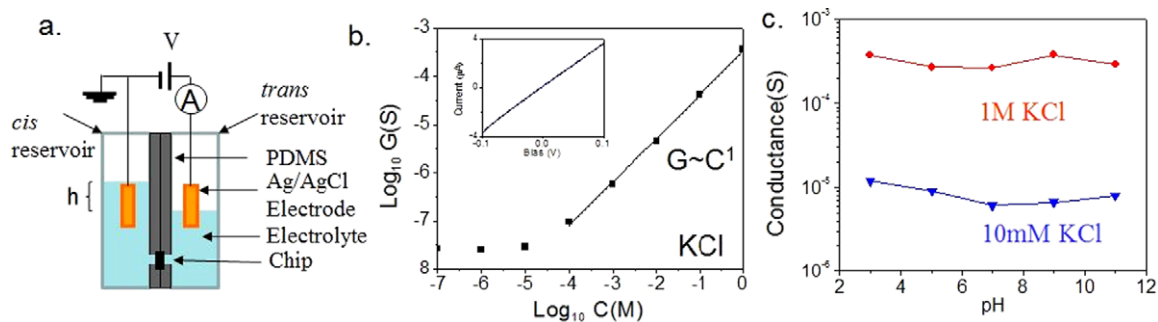
Figure 2. (a) Diagram of the ionic current measurement setup. *h* is the solution height difference between two reservoirs. (b) The ionic conductance versus KCl concentration on a log–log scale. The solid line is a linear fit to the experimental data. The inset shows the *I–V* curve of the membrane in 100 mM KCl solution. (c) The ionic conductance through the membrane as a function of pH in 1 M KCl (red circle) and 10 mM KCl (blue triangle) solutions. The solid lines are guides for the eye.

Purelab system, ELGA/Siemens). For some measurements, the water was further purified using a double-distillation system. The prepared salt solution was filtered through a 0.2 μm filter and degassed by sonication. For comparison, we also used anodic aluminum oxide (AAO) nanoporous membranes (Anodisc, Whatman) with pores of nominal diameter 20 nm and thickness of 60 μm. The AAO membrane was placed on the same silicon chip with a small opening in the center. The porosity of the AAO membrane is 25–50% of the total exposed surface area.

2.4. Measurement

The experimental setup is shown in figure 2(a). The fabricated CNT forest membrane is sandwiched between two flat polydimethylsiloxane (PDMS) slabs with punched holes (∼1 mm diameter) as fluid pathways. The sandwich structure is further clamped between two polystyrene optical cuvettes with 1 mm diameter fluid holes. The measurement setup is placed in a home-built Faraday cage to reduce noise. Bias is applied through Ag/AgCl electrodes (prepared by dipping clean 0.25 mm diameter Ag wire into bleach to a distance of 3–4 cm for 30 min) across the membrane at a fixed distance (∼1.2 cm). The applied bias is mostly below 2 V and never above 3 V to avoid water electrolysis, electrode polarization, and electric potential damage to molecules. The measurement is carried out at room temperature (∼22 C). No temperature change in solution is observed when applying 3 V for 2 h across the CNT membrane. The *cis* side is always grounded and the applied bias is defined as positive when the potential at the *trans* side is more positive. The analytes are always added on the *cis* side. The ionic current data are collected with a Keithley 2636 A (Keithley Instruments, Cleveland, OH). All the measurements are performed at room temperature. The electrical resistance of the fluidic pathway (without the membrane) is at least one order smaller than the resistance of the CNT membrane (see figure S3(b) in supplementary information available at stacks.iop.org/Nano/23/455101/mmedia). A pressure gradient is introduced by adjusting the height difference between the water surface level in *cis* and *trans* reservoirs. No obvious change in the height difference is observed for a 10 h experiment. The measured

ionic current of the same device is normally stable for weeks if the membrane is rinsed properly and stored in water all the time.

The concentration of permeates at the *trans* reservoir is measured by a UV–vis spectrometer (Ocean Optics, USB2000+ or Shimadzu UV1700 spectrometer) and square wave voltammetry (CH Instruments, CHI 760D).

3. Results and discussion

We have carried out several control experiments to prove that, within our applied bias and pressure range, the transport is through the inside of the CNT and not through the cracks and voids in the parylene film. We measured the ionic current through the membrane by using the setup as shown in figure 2(a). When control devices with pure parylene thin film are fabricated and treated by the same process (see section 2), no ionic current is measured. When the CNT membrane is not treated by oxygen plasma, there is no measurable ionic current. With the increase of the oxygen plasma time, the measured ionic current initially increases and then flattens out (see supplementary information available at stacks.iop.org/Nano/23/455101/mmedia). The dependence of ionic current on oxygen plasma time implies the ionic current is proportional to the number of opened CNTs in the membrane. We also studied the translocation of gold nanoparticles with well defined size under pressure and electric field. The 5 nm Au NP is smaller than the average CNT inner diameter and the 10 nm Au NP is larger than the average CNT inner diameter. We have measured more than 10 membranes and about 80% of the membranes only allow 5 nm Au NPs to pass with only electric field applied (see one example in figure 4(b)). However, the ratio is reduced to about 40% when a pressure (294 Pa, about 3 cm height difference) is applied. We discard the 60% membranes that also allow the passage of 10 nm NPs. This fact also suggests that these parylene encapsulated CNT membranes are not suitable for high pressure applications. Therefore, we mainly study the transport driven by electrical field. If a pressure gradient is needed, the pressure is always below 294 Pa, a level at which no leaks are detected in the parylene membranes.
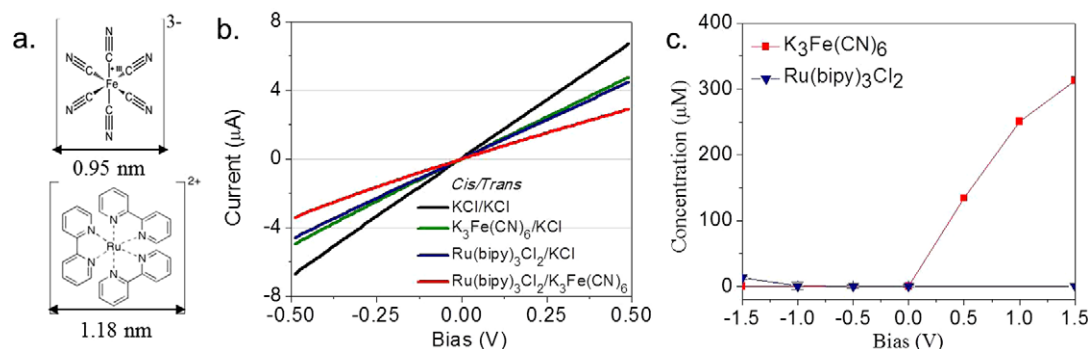
Figure 3. (a) Schemes of the molecular structure of the $Fe(CN)_6^{3-}$ anion and $Ru(bipy)_3^{2+}$ cation and their hydrated diameters. (b) The measured *I–V* curves when the *cis* and *trans* reservoirs are filled with KCl/KCl (black curve), $K_3Fe(CN)_6$/KCl (green curve), $Ru(bipy)_3Cl_2$/KCl (blue curve) and $Ru(bipy)_3Cl_2/K_3Fe(CN)_6$ (red curve), respectively. The concentration of KCl solution is 75 mM and the concentration of $Fe(CN)_6^{3-}$ anion and $Ru(bipy)_3^{2+}$ cation is 12.5 and 25 mM respectively. (c) The concentration of $Fe(CN)_6^{3-}$ anion (red square) and $Ru(bipy)_3^{2+}$ cation (blue triangle) at the *trans* reservoir as a function of the applied bias. The time is always 90 min. The solid lines are guides for the eye.

To understand the ion transport mechanisms in these large diameter MWCNTs, we measured the ionic conductance in KCl solution as a function of KCl concentration and solution pH. We first measured the ionic current through the CNT forest membrane at different bias. The current–voltage (*I–V*) curves are symmetric in the applied bias range (<2 V), and a typical curve taken in 100 mM KCl solution is shown in the inset of figure 2(b). The ionic conductance can be derived from the slope of the *I–V* curve. We then plot the ionic conductance data as a function of KCl concentration in a logarithmic scale. As shown in figure 2(b), the ionic conductance is proportional to the KCl concentration when it is above 0.1 mM. A deviation is observed when the concentration is below 0.1 mM. The deviation at low salt concentration was previously explained by surface charge on the nanochannel/nanopore [30]. However, the conductance departs from a linear relationship at much higher salt concentration (>10 mM) for silica nanochannels with surface charge density ~ 60 mC m^{-2} at pH 7. Even for an octadecyltrichlorosilane (OTS) modified silica channel with significantly reduced surface charge density, the deviation appears at around 1 mM KCl concentration [30]. Therefore, we concluded that the surface charge density at the inner surface of MWCNTs is extremely low. The proportionality at KCl concentration 0.1 mM–1 M suggests that the transport mechanism under electric field is electrophoresis. This is very different from the transport mechanism in individual SWCNTs with inner diameter below 2 nm [24, 15]. A unique power law relationship with exponent smaller than 1 is always observed in these single SWCNT fluidic devices. The origin of such behavior is attributed to the strong electroosmotic flow inside smaller diameter SWCNTs. We further studied the ionic conductance as a function of pH and the result is shown in figure 2(c). We did not observe any obvious change in ionic conductance when changing the pH of the KCl solution (both 1 M and 10 mM concentrations) from 3 to 9, which is very different from the results for small diameter SWCNTs. This result confirms the low surface charge density at the MWCNT inner surface and low net charge density of KCl

solution inside the MWCNTs. The following are possible reasons why the surface charge density is low at the inner surface of the MWCNTs. (1) Because of the inert nature of CNT inner surface, there are very few charged groups at the CNT inner surface. Charged groups (i.e. carboxyl groups) distribute mostly at the CNT ends. (2) The CNT inner surface may also acquire charges due to polarization when contacting charged solution or being affected by nearby environmental charges. However, the net charge density of the solution inside the large diameter MWCNT is low, as we discussed before. In addition, the conducting outer layers of MWCNTs can effectively screen the environmental charges. In summary, the electroosmotic flow is much weaker in these MWCNTs of 7 nm average diameter compared with small diameter SWCNTs. Due to the low surface charge, ion enrichment and ion depletion are not expected in our system [42, 25]. Electrophoresis will be the dominant transport mechanism. This conclusion is also consistent with previous experiments and theoretical calculations [33, 19]. It worth noting that increased electroosmotic flow has been observed by grafting small charged molecules at the inner surface of MWCNTs [36]. However, such modification will also increase the roughness of the CNT inner surface and a decrease in slip length is expected.

We then studied the transport of small molecules through these membranes. $Fe(CN)_6^{3-}$ anions (hydrated diameter $\sim$ 0.95 nm) [4] and $Ru(bipy)_3^{2+}$ cations (hydrated diameter $\sim$ 1.18 nm) [4] were used in this study. The molecular structures of both ions are shown in figure 3(a). We first measured the *I–V* curves and the results are shown in figure 3(b). The solutions in the *cis/trans* reservoirs are $K_3Fe(CN)_6$/KCl, $Ru(bipy)_3Cl_2$/KCl and $Ru(bipy)_3Cl_2/K_3Fe(CN)_6$. The KCl solution concentration is always 75 mM and the $K_3Fe(CN)_6$ and $Ru(bipy)_3Cl_2$ solutions are always 12.5 and 25 mM, which keeps the solution ionic strength at both reservoirs the same ($Ic = 1/2 \sum c_i Z_i^2$). As shown in figure 3(b), at the same bias (i.e. 0.25 V), the ionic current magnitude is in the following sequence: [KCl/KCl] > [$K_3Fe(CN)_6$/KCl] > [$Ru(bpy)_3Cl_2$/KCl] > [$Ru(bpy)_3Cl_2/K_3Fe(CN)_6$]. The same
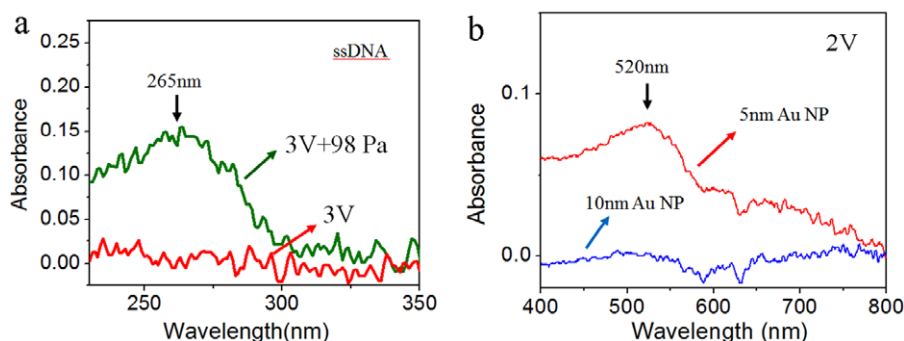
Figure 4. (a) UV–vis spectra of 12mer ssDNA at the *trans* reservoir after applying 3 V bias (red) and after applying 3 V bias and 98 Pa pressure simultaneously for 60 min (green). The solution in the *cis* reservoir is 5 μM ssDNA in 100 mM KCl solution. (b) UV–vis spectra of 5 nm (red) and 10 nm (blue) Au nanoparticles at the *trans* reservoir after applying a 2 V bias for 6 h. No pressure is applied. The concentration of Au NPs at the *cis* reservoir is 60 μM in 1 mM KCl solution.

sequence is observed for all the MWCNT membranes we measured. In order to verify the CNT effect, we also performed *I–V* measurements without the presence of MWCNT membrane in the ionic pathway. The measured ionic current magnitude at the same bias (i.e. 0.25 V) is in the following sequence: [KCl/KCl] > [Ru(bpy)$_3$Cl$_2$/KCl] > [K$_3$Fe(CN)$_6$/KCl] > [Ru(bpy)$_3$Cl$_2$/K$_3$Fe(CN)$_6$] (see figure S3(a) in supplementary information available at stacks.iop.org/Nano/23/455101/mmedia). The switch of sequence between Ru(bpy)$_3$Cl$_2$/KCl and K$_3$Fe(CN)$_6$/KCl with and without the presence of MWCNT membrane suggests that the Ru(bipy)$_3^{2+}$ cation passes the MWCNT membrane less easily, reflecting the extra interactions between the Ru(bipy)$_3^{2+}$ cation and the CNT inner surface (see further discussion in the next paragraph).

Here the ionic current is contributed by the transport of all the ion species in the solution. In order to study the transport of individual ions, we also directly measure the concentration of translocated ions at the *trans* reservoir after applying a bias between two reservoirs for 90 min. In this experiment, the *cis* reservoir is filled with 25 mM K$_3$Fe(CN)$_6$ or Ru(bipy)$_3$Cl$_2$ in 100 mM KCl (pH 7) solution. The *trans* reservoir is filled with 100 mM KCl solution. The concentration of Fe(CN)$_6^{3-}$ ions is determined by the pronounced redox peak at 0.18 V versus Ag/AgCl in square wave voltammetry. The concentration of Ru(bipy)$_3^{2+}$ ions is determined by the two adsorption peaks at 285 and 450 nm in UV–vis spectra. As shown in figure 3(c), the anion Fe(CN)$_6^{3-}$ can only be driven across the membrane by positive bias and the cation Ru(bipy)$_3^{2+}$ can only be driven across the membrane by negative bias. In addition, the concentration of transported ion increases with the applied bias. At zero bias, the concentration of transported ions is not detectable, confirming that diffusive transport is inefficient for these membranes. These results are consistent with the electric field induced electrophoretic transport. Of the two ions, the anion Fe(CN)$_6^{3-}$ is apparently much easier to transport through the MWCNTs and the concentration is about 25 times higher at the *trans* reservoir when the bias magnitude of 1.5 V is applied for 90 min between the two reservoirs. This observation is consistent with the *I–V* curves in figure 3(b). What is the reason for the large difference in

transport between anion Fe(CN)$_6^{3-}$ and cation Ru(bipy)$_3^{2+}$? Interestingly, the much higher rejection of cation Ru(bipy)$_3^{2+}$ than anion Fe(CN)$_6^{3-}$ is opposite to the observation in small diameter DWCNTs [4], in which the anion is rejected by the negatively charged carboxyl groups at the CNT ends. Because of the much larger diameter of MWCNTs in these membranes, the charges carried by the ions and at the CNT ends are likely fully screened by the electric double layer (EDL) at 100 mM KCl concentration. Therefore, the electrostatic interactions between ions and CNT ends are not important. In addition, the hydrated diameter of the Fe(CN)$_6^{3-}$ anion is only slightly smaller than that of the Ru(bipy)$_3^{2+}$ cation. So size induced steric hindrance will not contribute significantly to such obvious ion selectivity. One reason may be the different bulk electrophoretic mobility between Fe(CN)$_6^{3-}$ ($\sim$10.4 $\times$ 10^{-8} m^2 s^{-1} V^{-1}) and Ru(bipy)$_3^{2+}$ ($\sim$4.0 $\times$ 10^{-8} m^2 s^{-1} V^{-1}). However, the mobility of Fe(CN)$_6^{3-}$ is only about 2.5 times higher than the mobility of Ru(bipy)$_3^{2+}$, which cannot account for the 25-fold concentration difference at the *trans* reservoir. The main reason may be the stronger molecular interaction between the cation Ru(bipy)$_3^{2+}$ and the curved CNT inner surface. The origin of the interaction may be van der Waals forces and pi–pi stacking between the rings of the Ru(bipy)$_3^{2+}$ cation and the CNT inner surface. We also compared the transport between the anion Fe(CN)$_6^{3-}$ and cation Ru(bipy)$_3^{2+}$ through a nominal 20 nm pore diameter AAO membrane, and the difference is still obvious but much smaller (see figure S3 available at stacks.iop.org/Nano/23/455101/mmedia). This control experiment supports the view that the ion selectivity in the CNT membrane is mainly due to surface interactions.

We also studied the transport of DNA through these membranes. Theoretical simulations have made predictions that single-stranded DNA can pass through a CNT under external electric field [39, 6]. The translocation of short single-stranded DNAs through SWCNTs has also been reported [10, 29]. TEM revealed clear images of ssDNAs inside SWCNTs, which were injected by electrical field [13]. Interestingly, the ionic current signatures during DNA translocation in individual SWCNTs are quite different from
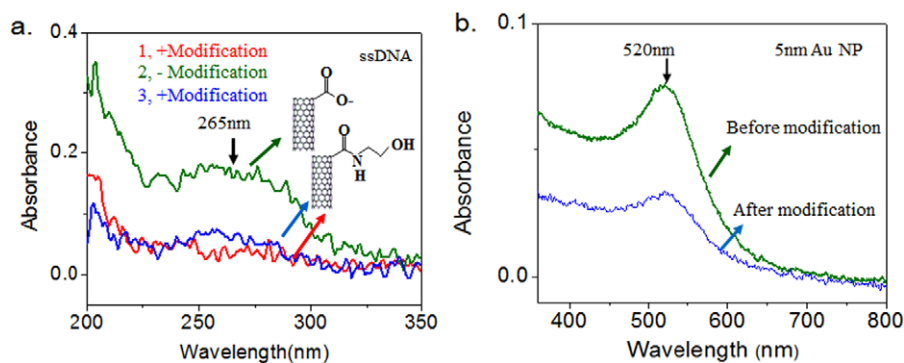
Figure 5. (a) UV–vis spectra of 12mer ssDNA at the *trans* reservoir after applying 147 Pa (1.5 cm water height difference) for 120 min for the membrane after ethanolamine modification (red), after removing the modification by oxygen plasma (green) and after ethanolamine modification again (blue). The initial concentration of ssDNA at the *cis* reservoir is 5 μM. (b) UV–vis spectra of 5 nm Au NPs in 1 mM KCl at the *trans* reservoir before (green) and after (blue) ethanolamine modification. The concentration of Au NPs at the *cis* reservoir is 10 μM in 1 mM KCl solution. A pressure of 147 Pa is applied for 36 min.

those in silicon based nanopores/nanochannels [14, 10, 12]. There are still no studies on the transport of DNA though large diameter MWCNT membranes. Here, we investigated the translocation of a 12mer ssDNA (GTCGTCGTCGTC) through the MWCNT membrane. As shown in figure 4(a), no DNA is detected in the UV–vis spectrometer at the *trans* reservoir when a bias of 3 V is applied across the membrane for 60 min. The same magnitude of bias is also applied for a longer time (>120 min) and still no DNA is detected by the UV–vis spectrometer. The DNA may be driven through the MWCNT membrane at a bias higher than 3 V. However, electrode polarization and water hydrolysis prevent studies at a higher bias. The difficulty of transporting ssDNA through these MWCNT membranes is probably due to (1) the strong interactions between the CNT inner surface and ssDNA, and (2) the lack of electroosmosis in these large diameter MWCNTs. It has been well studied that ssDNA will adsorb strongly to the CNT outer surface due to hydrophobic interaction and pi–pi stacking of DNA bases on the CNTs [40]. Molecular dynamics simulations [6], transmission electron microscopy (TEM) studies [23, 29] and dynamics force microscopy [16] also suggest DNA interacts with the CNT inner surface through hydrophobic and van der Waals forces. Therefore, without the efficient electroosmotic pumping, the moderate applied electric field is likely not enough to overcome the interaction force between the ssDNA and the CNT inner surface and cannot drive ssDNA through the large diameter MWCNTs. To test this hypothesis, we increase the driving force by adding a small pressure difference (98 Pa) between the two reservoirs. As the green curve shows in figure 4(a), ssDNA is detected at the *trans* reservoir. We also studied the electrophoretic transport of negatively charged 5 nm gold nanoparticles. As shown in figure 3(b), 5 nm gold nanoparticles can be detected at the *trans* reservoir by the UV–vis spectrometer after applying a 2 V bias across the membrane for 6 h. Although a 5 nm gold nanoparticle has larger size than 12mer ssDNA, the interaction between gold NPs and the CNT surface is presumably weaker than that for ssDNA due to the citrate coating on the surface of the gold NPs. Therefore, 5 nm gold NPs are easier to transport

through the MWCNT membrane. These results suggest the interactions between particles and the hydrophobic CNT inner surface strongly affect their electrophoretic transport through these large diameter MWCNT membranes.

Finally, we studied how chemical modification of CNT membranes affects particle transport. The chemical modification at the CNT ends may affect the particle transport by steric hindrance, electrostatic interactions and chemical bonding. During the fabrication, the CNT ends acquire carboxylate groups due to the oxygen plasma process. A variety of chemical modifications on the CNT ends can be easily accomplished by using well established carbodiimide chemistry to couple the carboxylic acid group with the amine group. Similar to previous reports [18, 15], a very simple molecule, ethanolamine, is used to modify the membrane, which will neutralize the negatively charged carboxyl groups (when pH > 4) and may hinder the particle transport at the pore entrance. Schematic diagrams of the unmodified and modified CNT ends are shown in the inset of figure 5(a). We first measured ionic current through these MWCNT membranes before and after the chemical modification in KCl solution. No difference in the ionic current was observed (see figure S4 available at stacks.iop.org/Nano/23/455101/mmedia). This suggests that the modification does not affect the transport of small ions, such as K$^+$ and Cl$^-$. We then measured the transport of larger particles, including 12mer ssDNA (GTCGTCGTCGTC) and 5 nm gold NPs under a small pressure (∼147 Pa). The results are shown in figure 5. The transport of ssDNA and 5 nm diameter gold NPs across the membrane is obviously suppressed by the ethanolamine modification (blue curves in figures 5(a) and (b)). The observed effect is most likely due to steric hindrance, because there is no charge on the CNT ends after modification. To further confirm the chemical modification effect, we use oxygen plasma to remove the modified molecules and then redo the modification. As shown in figure 5(a), the transport of ssDNA across the CNT membrane is correspondingly recovered (green curve) and then hindered (blue curve). Here we just use a simple molecule to demonstrate the capability of reversible chemical modification on these

parylene embedded MWCNT membranes. By using rationally designed molecules, we expect to enhance selectivity and electroosmotic flow in these MWCNT membranes [32]. Here, the ethanolamine molecules mainly modified the CNT ends. The grafting of rationally designed charged molecules inside the CNT will be another way to enhance the selectivity.

4. Conclusions

In summary, we have successfully fabricated parylene encapsulated vertically aligned large diameter MWCNT membranes. In contrast to small diameter DWCNTs and SWCNTs, electroosmosis in these large diameter MWCNTs is weak. Therefore, an electric field can only provide a weak force to drive ions and small molecules. The transport is also significantly affected by the interactions with the hydrophobic CNT inner surface, leading to enhanced selectivity for small molecules. Chemical modification on these MWCNT membranes also shows an obvious effect on the translocation of particles.

Acknowledgments

References

[1] Cai D *et al* 2010 A molecular-imprint nanosensor for ultrasensitive detection of proteins *Nature Nanotechnol.* **5** 597–601

[2] Corry B 2007 Designing carbon nanotube membranes for efficient water desalination *J. Phys. Chem.* B **112** 1427–34

[3] Derylo M A, Morton K C and Baker L A 2011 Parylene insulated probes for scanning electrochemical-atomic force microscopy *Langmuir* **27** 13925–30

[4] Fornasiero F, Park H G, Holt J K, Stadermann M, Grigoropoulos C P, Noy A and Bakajin O 2008 Ion exclusion by sub-2 nm carbon nanotube pores *Proc. Natl Acad. Sci. USA* **105** 17250–5

[5] Gao C, Ding S, Tan Q and Gu L-Q 2008 Method of creating a nanopore-terminated probe for single-molecule enantiomer discrimination *Anal. Chem.* **81** 80–6

[6] Gao H, Kong Y, Cui D and Ozkan C S 2003 Spontaneous insertion of DNA oligonucleotides into carbon nanotubes *Nano Lett.* **3** 471–3

[7] Hinds B J, Chopra N, Rantell T, Andrews R, Gavalas V and Bachas L G 2004 Aligned multiwalled carbon nanotube membranes *Science* **303** 62–5

[8] Holt J K, Park H G, Wang Y M, Stadermann M, Artyukhin A B, Grigoropoulos C P, Noy A and Bakajin O 2006 Fast mass transport through sub-2 nm carbon nanotubes *Science* **312** 1034–7

[9] Hummer G, Rasaiah J C and Noworyta J P 2001 Water conduction through the hydrophobic channel of a carbon nanotube *Nature* **414** 188–90

[10] Karnik R, Fan R, Yue M, Li D, Yang P and Majumdar A 2005 Electrostatic control of ions and molecules in nanofluidic transistors *Nano Lett.* **5** 943–8

[11] Lee C Y, Choi W, Han J-H and Strano M S 2010 Coherence resonance in a single-walled carbon nanotube ion channel *Science* **329** 1320–4

[12] Li J, Stein D, McMullan C, Branton D, Aziz M J and Golovchenko J A 2001 Ion-beam sculpting at nanometre length scales *Nature* **412** 166–9

[13] Li Y, Chen S, Kaneko T and Hatakeyama R 2011 Electrically moving single-stranded DNA into and out of double-walled carbon nanotubes *Chem. Commun.* **47** 2309–11

[14] Liang X and Chou S Y 2008 Nanogap detector inside nanofluidic channel for fast real-time label-free DNA analysis *Nano Lett.* **8** 1472–6

[15] Liu H, He J, Tang J, Liu H, Pang P, Cao D, Krstic P, Joseph S, Lindsay S and Nuckolls C 2010 Translocation of single-stranded DNA through single-walled carbon nanotubes *Science* **327** 64–7

[16] Lulevich V, Kim S, Grigoropoulos C P and Noy A 2011 Frictionless sliding of single-stranded DNA in a carbon nanotube pore observed by single molecule force spectroscopy *Nano Lett.* **11** 1171–6

[17] Majumder M, Chopra N, Andrews R and Hinds B J 2005 Nanoscale hydrodynamics: enhanced flow in carbon nanotubes *Nature* **438** 44

[18] Majumder M, Chopra N and Hinds B J 2005 Effect of tip functionalization on transport through vertically oriented carbon nanotube membranes *J. Am. Chem. Soc.* **127** 9062–70

[19] Majumder M, Chopra N and Hinds B J 2011 Mass transport through carbon nanotube membranes in three different regimes: ionic diffusion and gas and liquid flow *ACS Nano* **5** 3867–77

[20] Mattia D and Gogotsi Y 2008 Review: static and dynamic behavior of liquids inside carbon nanotubes *Microfluid. Nanofluid.* **5** 289–305

[21] Miserendino S, Yoo J, Cassell A and Tai Y-C 2006 Electrochemical characterization of parylene-embedded carbon nanotube nanoelectrode arrays *Nanotechnology* **17** S23

[22] Noy A, Park H G, Fornasiero F, Holt J K, Grigoropoulos C P and Bakajin O 2007 Nanofluidics in carbon nanotubes *Nano Today* **2** 22–9

[23] Okada T, Kaneko T, Hatakeyama R and Tohji K 2006 Electrically triggered insertion of single-stranded DNA into single-walled carbon nanotubes *Chem. Phys. Lett.* **417** 288–92

[24] Pang P, He J, Park J H, Krstić P S and Lindsay S 2011 Origin of giant ionic currents in carbon nanotube channels *ACS Nano* **5** 7277–83

[25] Pu Q, Yun J, Temkin H and Liu S 2004 Ion-enrichment and ion-depletion effect of nanochannel structures *Nano Lett.* **4** 1099–103

[26] Qin X, Yuan Q, Zhao Y, Xie S and Liu Z 2011 Measurement of the rate of water translocation through carbon nanotubes *Nano Lett.* **11** 2173–7

[27] Schoch R B, Han J and Renaud P 2008 Transport phenomena in nanofluidics *Rev. Mod. Phys.* **80** 839

[28] Scott M *et al* 2006 Electrochemical characterization of parylene-embedded carbon nanotube nanoelectrode arrays *Nanotechnology* **17** S23

[29] Shoda M, Bandow S, Maruyama Y and Iijima S 2009 Probing interaction between ssDNA and carbon nanotubes by

Raman scattering and electron microscopy *J. Phys. Chem.* C **113** 6033–6

[30] Stein D, Kruithof M and Dekker C 2004 Surface-charge-governed ion transport in nanofluidic channels *Phys. Rev. Lett.* **93** 035901

[31] Strano M S, Dyke C A, Usrey M L, Barone P W, Allen M J, Shan H, Kittrell C, Hauge R H, Tour J M and Smalley R E 2003 Electronic structure control of single-walled carbon nanotube functionalization *Science* **301** 1519–22

[32] Sun X, Su X, Wu J and Hinds B J 2011 Electrophoretic transport of biomolecules through carbon nanotube membranes *Langmuir* **27** 3150–6

[33] Thomas J A and McGaughey A J H 2008 Reassessing fast water transport through carbon nanotubes *Nano Lett.* **8** 2788–93

[34] Wang Z, Ou Y, Lu T-M and Koratkar N 2007 Wetting and electrowetting properties of carbon nanotube templated parylene films *J. Phys. Chem.* B **111** 4296–9

[35] Whitby M and Quirke N 2007 Fluid flow in carbon nanotubes and nanopipes *Nature Nanotechnol.* **2** 87–94

[36] Wu J, Gerstandt K, Majumder M, Zhan X and Hinds B J 2011 Highly efficient electroosmotic flow through functionalized carbon nanotube membranes *Nanoscale* **3** 3321–8

[37] Wu J, Gerstandt K, Zhang H, Liu J and Hinds B J 2012 Electrophoretically induced aqueous flow through single-walled carbon nanotube membranes *Nature Nanotechnol.* **7** 133–9

[38] Wu J, Paudel K S, Strasinger C, Hammell D, Stinchcomb A L and Hinds B J 2010 Programmable transdermal drug delivery of nicotine using carbon nanotube membranes *Proc. Natl Acad. Sci. USA* **107** 11698–702

[39] Xie Y, Kong Y, Soh A K and Gao H 2007 Electric field-induced translocation of single-stranded DNA through a polarized carbon nanotube membrane *J. Chem. Phys.* **127** 225101

[40] Zheng M *et al* 2003 Structure-based carbon nanotube sorting by sequence-dependent DNA assembly *Science* **302** 1545–8

[41] Zhong G, Warner J H, Fouquet M, Robertson A W, Chen B and Robertson J 2012 Growth of ultrahigh density single-walled carbon nanotube forests by improved catalyst design *ACS Nano* **6** 2893–903

[42] Zhou K, Kovarik M L and Jacobson S C 2008 Surface-charge induced ion depletion and sample stacking near single nanopores in microfluidic devices *J. Am. Chem. Soc.* **130** 8614–6